PAPER

Check for updates

Cyano-functionalized pyrazine: an electron-deficient unit as a solid additive enables binary organic solar cells with 19.67% efficiency†

Lijun Tu,[a] Hao Wang,[a] Weixu Duan,[b] Ruijie Ma, [ID] *[c] Tao Jia,[d] Top Archie Dela Peña, [ID] [ef] Yongmin Luo,[e] Jiaying Wu, [ID] [e] Mingjie Li,[f] Xiaomin Xia,[a] Siqi Wu,[a] Kai Chen,*[b] Yue Wu, [ID] [g] Yulin Huang,[hi] Kun Yang,[hi] Gang Li [ID] *[c] and Yongqiang Shi [ID] *[a]

Additive engineering has been regarded as a valuable approach for enhancing the power conversion efficiencies (PCEs) of organic solar cells (OSCs). However, the effective solid additive molecules, especially electron-deficient building blocks, that enhance the PCEs of OSCs are still limited. Herein, two cyano-functionalized highly electron-deficient building blocks, namely 3,6-dibromopyrazine-2-carbonitrile (CNPz) and 3,6-dibromopyrazine-2,5-dicarbonitrile (DCNPz), which feature simple structures and facile synthesis are employed as solid additives to optimize the performance of OSCs. It is found that CNPz can modulate the intermolecular interactions and improve the molecular packing, which is beneficial for charge generation, transport, and collection. As a result, a 19.67% PCE is achieved in the PTQ10/*m*-BTP-PhC6 binary devices, ranking amongst the highest values for OSCs. Furthermore, the general applicability of solid additives is demonstrated in other organic photovoltaic systems. These findings offer valuable insights into designing and developing novel electron-deficient solid additives to boost the efficiency of OSCs.

Broader context

Bulk-heterojunction (BHJ) organic solar cells (OSCs) have gained considerable attention from academia and industry due to their advantages, such as low-cost, lightweight, solution processability, and flexibility. Incorporating solid additives into the active layer is recognized as an effective strategy to optimize the nanoscale morphology and enhance efficiency. Most of the previously reported solid additives are based on benzene or thiophene units. However, the introduction of an electron-deficient acceptor unit as a solid additive in OSCs remains largely unexplored. Driven by these unstudied phenomena, we designed and synthesized two cyano-functionalized pyrazine building blocks, namely 3,6-dibromopyrazine-2-carbonitrile (CNPz) and 3,6-dibromopyrazine-2,5-dicarbonitrile (DCNPz). These two building blocks have simple structures, and their synthesis is straightforward. CNPz and DCNPz can be synthesized *via* only one-step reaction and three-step reactions from cheap raw materials, respectively, making them much more easily accessible than electron-rich units. Consequently, the PCE of the PTQ10/*m*-BTP-PhC6-based device is significantly boosted from 18.73% to 19.67% with a significant increase of the J_{SC} and FF (81.8%) *via* a CNPz additive strategy. These findings offer valuable insights into designing and developing novel electron-deficient solid additives to boost the efficiency of OSCs.

[a] Key Laboratory of Functional Molecular Solids, Ministry of Education, and School of Chemistry and Materials Science, Anhui Normal University, Wuhu, Anhui 241002, China. E-mail: shiyq@ahnu.edu.cn

[b] Guangxi Key Lab of Processing for Nonferrous Metals and Featured Materials and Key lab of new Processing Technology for Nonferrous Metals and Materials, Ministry of Education, School of Resources, Environments and Materials, Guangxi University, Nanning 530004, China. E-mail: chenkai@gxu.edu.cn

[c] Department of Electrical and Electronic Engineering, Research Institute of Smart Energy (RISE), Photonic Research Institute (PRI), The Hong Kong Polytechnic University, Hung Hum Kowloon, Hong Kong 999077, China. E-mail: ruijie.ma@polyu.edu.hk, gang.w.li@polyu.edu.hk

[d] School of Optoelectronic Engineering, School of Mechanical Engineering, Guangdong Polytechnic Normal University, Guangzhou, 510665, China

[e] Advanced Materials Thrust, Function Hub, The Hong Kong University of Science and Technology, Nansha, Guangzhou, 511400, China

[f] Faculty of Science, Department of Applied Physics, The Hong Kong Polytechnic University, Kowloon, Hong Kong, 999077, P. R. China

[g] Laboratory of Advanced Optoelectronic Materials, Suzhou Key Laboratory of Novel Semiconductor-Optoelectronics Materials and Devices, College of Chemistry Chemical Engineering and Materials Science, Soochow University, Jiangsu, Suzhou 215123, China

[h] State Key Laboratory of Chemo/Biosensing and Chemometrics, College of Chemistry and Chemical Engineering, Hunan University, Changsha 410082, China

[i] Shenzhen Research Institute of Hunan University, Shenzhen 518000, China

† Electronic supplementary information (ESI) available. See DOI: https://doi.org/10.1039/d4ee00764f

This journal is © The Royal Society of Chemistry 2024

Energy Environ. Sci., 2024, **17**, 3365–3374 | 3365

Introduction

Bulk-heterojunction (BHJ) organic solar cells (OSCs) emerging as a significant renewable green energy technology have attracted enormous attention due to their numerous advantages, including light weight, solution processability, and flexibility.[1–12] In the past few years, many efforts have been devoted to improving the PCE of organic photovoltaics (OPV), including designing and synthesizing new non-fullerene small molecule acceptors (NFSMAs) and polymer donors,[13–28] employing various charge-transporting layers, and optimizing the device architecture. Thanks to these efforts, power conversion efficiencies (PCEs) of over 19% have been achieved in single-junction OSCs.[29–34] Besides the innovation in the design of new donor and acceptor organic semiconductor materials, rationally tuning the morphology of the active layer is also crucial to maximize the PCE of OSCs.[35–42]

Recently, various approaches have been explored to optimize the morphology of active layers, such as thermal annealing, the introduction of a third component, and additive strategies, *etc.*[43–47] Among these methods, utilizing additive molecules to adjust the intermolecular interactions of active layers has been demonstrated to be a facile and efficient method to improve charge-carrier transport and collection.[48–51] Traditional liquid additives, such as 1-chloronaphthalene (CN) and 1,8-diiodooctane (DIO), have been widely used to optimize the device performance.[52,53] Compared to limited efforts and success on the design and synthesis of liquid additives, there seems to be great room for developing new solid additives to manipulate the active layer morphology to improve the device performance.

Volatile solid additives (VSAs) have emerged as a facile and effective approach to tailor the film morphology through the molecular interactions with the donor and acceptor, thus significantly improving the device performance. More importantly, VSA can be completely removed from the active layer through thermal treatment, thus resulting in the OSCs typically having better reproducibility and long-term operational stability compared to the devices processed by solvent additives with high boiling point. For example, Hou *et al.*[54–56] reported a series of solid

additives, which play a crucial role in enhancing the intermolecular interactions and molecular packing of the donor/acceptor blend and improving ordered π–π stacking and charge transport. Huang *et al.*[57] adopted the benzo[1,2-*b*:4,5-*b'*]dithiophene (BDT) to manipulate the morphology of PM6:L8-BO and achieved a PCE of over 19% by enhancing charge transport, exciton dissociation and collection as well as suppressing bimolecular recombination. Subsequently, various solid additives were developed yielding PCEs over 19% for binary or ternary device systems.[58–62] Although these solid additives have made significant breakthroughs in improving the device performance, it is still necessary to develop new solid additives to better understand the working mechanism. Most of the previously reported solid additives are based on benzene or thiophene units (Fig. 1(a) and (b)). The active layers of BHJ OSCs consist of hole- and electron-transporting materials. Compared to hole-transporting materials, nonfullerene small-molecule semiconductors (electron-transporting) often exhibit lower electron mobility, leading to unbalanced charge transport in the device. A possible solution is to enhance the electron mobility by introducing n-type solid additives, thereby facilitating more balanced charge transport, thus improving the device performance. However, the introduction of an electron-deficient acceptor unit as a solid additive in OSCs remains largely unexplored. A thorough investigation into this working mechanism is urgently needed. The number of electron-deficient units as solid additives in OSCs is limited because of the challenge of synthesizing molecules with favorable energies, good solubility, and high miscibility with the donor/acceptor.[63] Notably, only a handful of electron-deficient units have been successfully employed in OSCs, garnering a modestly increased PCE of just over 18%.[64] Therefore, it is strongly desired to develop new electron-deficient building blocks as solid additives to boost the PCE of OSCs.

Pyrazine as a strong electron-withdrawing unit has been widely used in organic semiconductors, particularly in organic thin-film transistors and organic thermoelectric fields. Its corresponding compounds showed high electron mobilities exceeding 1 cm² V⁻¹ s⁻¹.[65] Such strong acceptor units are highly pursued for developing high performance OSCs. In this work, we designed and synthesized two cyano-functionalized pyrazine

Fig. 1 Recent development of (a) thiophene and (b) benzene derivatives as additives in binary OSCs, and (c) our molecular chemical structures reported in this work.

building blocks, namely 3,6-dibromopyrazine-2-carbonitrile (CNPz) and 3,6-dibromopyrazine-2,5-dicarbonitrile (DCNPz).[65] These two building blocks have simple structures, and their synthesis is straightforward. CNPz and DCNPz can be synthesized *via* only one-step reaction and three-step reactions from cheap raw materials, respectively, making them much more easily accessible than electron-rich units. After systematically studying their thermal properties and molecular interactions with the donor/acceptor, they were incorporated into the PTQ10/*m*-BTP-PhC6 binary system to comprehensively investigate their effect on the BHJ morphology and photovoltaic performance of OSCs. The studies showed that the electronegative CNPz could interact with the electropositive main chain of polymer donor PTQ10, thus improving compact molecular packing and crystallinity for the blend film. Consequently, the PCE of the PTQ10/*m*-BTP-PhC6-based device is significantly boosted from 18.73% to 19.67% with a significant increase of the J_{SC} and FF (81.8%) *via* the CNPz additive strategy (Fig. 1(c)). As far as we know, pyrazine derivatives have not been used as solid additives in OSCs. This work highlights the importance of rational design of electron-deficient units as solid additives for high-performance OSCs.

Results and discussion

The chemical structures of polymer donor PTQ10, acceptor *m*-BTP-PhC6, and solid additives CNPz and DCNPz are shown in Fig. 2(a). CNPz and DCNPz can be synthesized *via* only one-step reaction and three-step reactions from cheap raw materials, respectively. The corresponding synthetic routes are provided in Scheme S1 (ESI†). The thermal properties of both solid additives were evaluated by thermogravimetry analysis (TGA) and differential scanning calorimetry (DSC). As shown in Fig. S10 (ESI†), the T_d (5% weight loss) values for CNPz and DCNPz are 170 °C and 210 °C, respectively, indicating that these additives can vaporize under high-temperature annealing conditions. This phenomenon was further confirmed through X-ray photoelectron spectroscopy (XPS). As shown in Fig. S11 (ESI†), the characteristic Br element peaks of PTQ10:*m*-BTP-PhC6 blend films without/with different solid additives were not observed after thermal annealing. DSC curves showed that their melting points are 110 °C and 210 °C for CNPz and DCNPz, respectively, indicating different intermolecular interactions in their solid state.

The electrostatic potential surfaces (ESP) of PTQ10, *m*-BTP-PhC6, CNPz and DCNPz were calculated by density functional theory (DFT). As shown in Fig. 2(b), the backbone of polymer donor PTQ10 shows an electronegativity ESP distribution on the surface. In contrast, the *m*-BTP-PhC6 molecule predominantly presents a positive ESP distribution on the surface, specifically in the BTP core unit. For CNPz and DCNPz additives, the electro-positivity of the pyrazine core leads to a distinct concentration of positive charge in the surrounding region. Thus, we speculate that CNPz/DCNPz could potentially

Fig. 2 (a) Chemical structures of polymer donor PTQ10, acceptor *m*-BTP-PhC6, and solid additives CNPz and DCNPz. (b) ESP distributions and dipole moments for PTQ10, *m*-BTP-PhC6, and the two solid additives.

interact with the conjugated backbone of the above polymer donor PTQ10 based on the opposite polarity attraction theory,[66] which could affect their molecular organization during the film-formation process. Additionally, the dipole moment of CNPz is 3.69 Debye, significantly higher than DCNPz (0.00002 Debye) and other reported solid additives. The higher dipole moment in CNPz implies a more robust intermolecular interaction with PTQ10. The intrinsic intermolecular interaction may affect the morphology and molecular stacking in the blend film, thus further influencing the device performance.

To further investigate the impact of the two solid additives on the intermolecular interactions with polymer donor PTQ10 and *m*-BTP-PhC6, the most energetically favorable conformations were accordingly required (Fig. 3). The CNPz additive tends to interact with the quinoxaline core of PTQ10, while DCNPz interacts with its adjacent thiophene ring. As for the contact site of the additives with *m*-BTP-PhC6, CNPz and DCNPz are inclined to the benzothiadiazole (BT) core. According to the optimal geometries, the binding energies (ΔG) between CNPz/DCNPz additives and PTQ10 or *m*-BTP-PhC6 were accordingly determined.[67,68] The ΔG_b values are calculated as -0.027 and -1.57 kcal mol^{-1} for the two dimers of CNPz:PTQ10 and DCNPz:PTQ10 with different bound conformations, respectively. Concerning the CNPz/DCNPz:*m*-BTP-PhC6 systems, the values of $\Delta G_{CNPz:m\text{-}BTP\text{-}PhC6}$ (-2.89 kcal mol^{-1}) and $\Delta G_{DCNPz:m\text{-}BTP\text{-}PhC6}$ (-4.37 kcal mol^{-1}) were recorded. These results further validate that the solid additives can construct and order molecular stacking of the donor and acceptor in OSCs.

To assess the impact of CNPz and DCNPz solid additives on the photovoltaic performance of the OSCs, devices with a conventional structure of ITO/PEDOT:PSS/active layer/PFN-Br/Ag were fabricated (Fig. 4(a)). Detailed fabrication procedures and optimization conditions are provided in the ESI.† The current density–voltage (J–V) curves and related photovoltaic parameters of the OSCs are summarized in Fig. 4(b) and

Table 1. The control device PTQ10:*m*-BTP-PhC6 yields a PCE of 18.73%. Upon the introduction of the CNPz additive, a significantly improved PCE of 19.67% was achieved, mainly in J_{SC} (27.29 mA cm^{-2}) and FF (81.8%) enhancement. So far, the PCE of 19.67% and FF of 81.8% are among the highest values for the binary solid additive processed OSCs, which are much higher than that of the electron-rich unit as additives in OSCs. A certified efficiency of 19.20% (Fig. S12, ESI†) was achieved by the South China National Center of Metrology-Guang Dong Institute of Metrology. However, for the DCNPz-processed device, a slightly lower PCE of 18.34% was obtained, which may be due to the restricted miscibility between the DCNPz and PTQ10:*m*-BTP-PhC6 system. The additive effect on the photovoltaic performance was further investigated by the external quantum efficiency (EQE) spectra (Fig. 4(c)). Compared to the control device, the CNPz-processed device delivers an elevated response with the maximum response over 85% at 550 nm, thus contributing to the J_{SC} enhancement. For the control device and CNPz/DCNPz-processed OSC, the integrated J_{SC} values from the EQE curves are 25.70, 26.36, and 25.47 mA cm^{-2}, respectively, which are in good agreement with the values obtained from the J–V curves. Meanwhile, 1,4-diiodobenzene (DIB) was chosen as the solid additive for comparison. According to the J–V curve in Fig. S13 (ESI†), the device showed a PCE of 18.00% with a V_{OC} of 0.882 V, a J_{SC} of 25.26 mA cm^{-2}, and an FF of 80.8%. The PCE is lower than that of the CNPz-processed PTQ10:*m*-BTP-PhC6 system, which may be due to the large phase separation induced by DIB. This phenomenon is negative for achieving abundant charge generation. This results suggest that rationally introducing electron-deficient building blocks as solid additives is an effective strategy to boost the photovoltaic performance of OSCs.

To further investigate the effect of solid additives on the device performance, photocurrent (J_{Ph}) *versus* effective voltage (V_{eff}) were plotted (Fig. 4(d)). Charge dissociation efficiency (P_{diss}) and collection efficiency (P_{coll}) were calculated. As shown

Fig. 3 The strongest conformations and calculated binding energies for the complexes of (a) PTQ10:CNPz, *m*-BTP-PhC6:CNPz and (b) PTQ10:DCNPz, *m*-BTP-PhC6:DCNPz.

Fig. 4 (a) Device structure for OSCs used in this work. (b) J–V curves of the control and CNPz/DCNPz-processed PTQ10:m-BTP-PhC6 OSCs. (c) EQE spectra of the control and CNPz/DCNPz-processed OSCs. (d) J_{ph}–V_{eff} curves. (e) Statistical PCE *versus* FF of the binary solid additive processed OSCs in previous reports and this work. (f) Charge carrier mobilities and hole/electron ratios of OSCs processed without/with CNPz and DCNPz additives. PL spectra and the corresponding quenching efficiency of the control (g), CNPz (h) and DCNPz (i)-processed PTQ10:m-BTP-PhC6 OSCs.

in Fig. 4(d), it is found that the J_{ph} of the CNPz-processed OSCs increases more rapidly and reaches saturation earlier, indicating that the CNPz-processed device has higher exciton dissociation and charge collection efficiencies. This implies that the ordered molecular packing and shortened π–π stacking preferentially optimize the charge collection process of the OSCs. Meanwhile, the dependences of J_{SC} and V_{OC} on light intensity (P_{light}) were further investigated and shown in Fig. S14 (ESI†). The slopes (α) of all devices are close to unity, suggesting that all OSCs possess relatively weak bimolecular recombination. Charge recombination and collection procedures are closely related to their charge transportation. Therefore, the space-charge-limited-current (SCLC) method was used to evaluate their hole ($μ_h$) and electron ($μ_e$) mobilities. As shown in Fig. 4(f) and Fig. S15 (ESI†), the blend films processed without

additive, and with CNPz and DCNPz showed $μ_h/μ_e$ of $5.06 \times 10^{-4}/3.11 \times 10^{-4}$, $6.44 \times 10^{-4}/4.02 \times 10^{-4}$, and $4.83 \times 10^{-4}/0.78 \times 10^{-4}$ cm^2 V^{-1} s^{-1}, respectively. Compared to the control device, the films processed with CNPz additive demonstrate higher charge mobilities and a more balanced electron and hole mobility, accounting for the highest values of J_{SC} and FF for the CNPz-processed OSCs. Furthermore, the blend film processed with CNPz additive exhibited the highest quenching efficiency (93.4%) of photoluminescence (PL, Fig. 4(h)), suggesting the most efficient charge generation.

To gain more insight into the effect of solid additives on the exciton dissociation and free charge recombination dynamic process of OSC, the photo-induced hole transfer and its decay dynamics from active layers were investigated by femtosecond transient absorption spectroscopy (fs-TAS).[69] The ground state

Table 1 Photovoltaic parameters of the PTQ10:m-BTP-PhC6 system processed without or with different solid additives

Solid additive	V_{OC} (V)	J_{SC} (mA cm^{-2})	Cal. J_{SC} (mA cm^{-2})	FF (%)	PCE (%)
w/o	0.883	26.55	25.70	79.9	18.73
	0.881 ± 0.05	26.32 ± 0.19		79.6 ± 0.4	18.35 ± 0.32
CNPz	0.884	27.20	26.36	81.8	19.67
	0.882 ± 0.04	27.04 ± 0.13		80.7 ± 0.5	19.40 ± 0.25
DCNPz	0.884	26.19	25.47	79.2	18.34
	0.880 ± 0.05	25.89 ± 0.28		78.5 ± 0.8	17.87 ± 0.39

This journal is © The Royal Society of Chemistry 2024

Energy Environ. Sci., 2024, **17**, 3365–3374 | **3369**

bleaching (GSB) signals of the pure films peaking at around 610 nm for PTQ10 singlets and also the visible-range features of *m*-BTP-PhC6 singlet excitons are shown in Fig. S16 and 17 (ESI†). The blend films were pumped under an 800 nm laser with 3 μJ cm^{-2} fluence to selectively excite the acceptor *m*-BTP-PhC6 forming singlet excitons which can undergo hole transfer dynamics towards PTQ10 and subsequently generating PTQ10 hole polarons. As shown in Fig. 5(a) and (b), the positive photobleach signal in the range of 500–640 nm indicates the ultrafast hole transfer process from *m*-BTP-PhC6 to PTQ10, consistent with the PTQ10 absorption spectrum. Meanwhile, the photobleaching intensity of PTQ10 hole polarons (500–640 nm) appears to increase, indicating a more favorable hole transfer from *m*-BTP-PhC6 to PTQ10. As depicted in Fig. S18 (ESI†), the CNPz additive-treated blend film demonstrated elevated $\Delta T/T$ value relative to the control one, suggesting attenuated charge recombination. It can then be inferred that CNPz-processed PTQ10:*m*-BTP-PhC6 achieved a more efficient charge generation due to more favorable hole transfer, thus leading to the significant elevation of J_{SC}.

To further investigate the effect of solid additives on the bend film morphologies, atomic force microscopy (AFM) and transmission electron microscopy (TEM) measurements were carried out. As shown in Fig. 6(a)–(c), PTQ10:*m*-BTP-PhC6 blend films exhibit similar morphology with homogeneous nanophase, and they have relatively smooth surfaces with root-mean-square roughness (RMS) values of 0.57, 0.56, and 0.54 nm for the control device, CNPz and DCNPz proceeded blend films, respectively. Similar to the blend films, CNPz and DCNPz can also modulate the film morphology of polymer donor PTQ10 (Fig. S19, ESI†). For the TEM images, the additives can also tune the phase separation. Compared to the control device PTQ10:*m*-BTP-PhC6 blend film (Fig. 6(d)), more fibrillar networks were obviously observed for the CNPz-processed blend film (Fig. 6(e)), indicating efficient charge transport within the

blend films. The better fiber structure for the CNPz-processed blend film implies that introducing CNPz additive to the PTQ10:*m*-BTP-PhC6 system is helpful to regulate the morphology and thus achieve high FF and PCE values.

Furthermore, 2D-grazing incidence wide angle X-ray scattering (2D-GIWAXS) measurements were performed to investigate the effect of solid additives on the crystallinity and molecular packing properties of PTQ10 and *m*-BTP-PhC6 as well as their blend films. The 2D-GIWAXS diffraction patterns are shown in Fig. 7(a)–(c) and Fig. S20, S21 (ESI†) and the corresponding 1D line cuts are depicted in Fig. 7(d) and (e). As shown in Fig. 7(a)–(c), it can be found that all the blend films showed obvious (010) π–π stacking peaks along the q_z direction (out-of-plane, OOP) and (100) diffraction along the q_{xy} direction (in-plane, IP), implying that the preferred face-on molecular orientations in the PTQ10:*m*-BTP-PhC6 blend films can be well maintained after different solid additive treatments. Compared to the control device, the CNPz-processed film showed a marginally smaller π–π stacking distance of 3.61 Å, indicating more compact molecular packing between the conjugated backbone. For the CNPz-processed blend film, the CCLs of the (010) peaks in the OOP direction increased from 16.7 Å to 17.5 Å, indicating enhanced crystallization ordering (Tables S1–S6, ESI†). These results indicate that CNPz-processed PTQ10:*m*-BTP-PhC6 blend film could enhance the molecular packing and improve the degree of crystallinity, which is beneficial for promoting the charge transport, resulting in boosted J_{SC} and FF.

The impacts of solid additives CNPz and DCNPz on the aggregation behaviors of PTQ10, *m*-BTP-PhC6, and PTQ10:*m*-BTP-PhC6 blend films were investigated by UV-vis measurement. As illustrated in Fig. S22 (ESI†), the reduced I_{0-1} ratios of the additive-processed PTQ10 films related to the pure PTQ10 film were observed, indicating diminished J-aggregation. However, the absorption spectra of the acceptor *m*-BTP-PhC6 films without/with CNPz/DCNPz processed are almost unchanged,

Fig. 5 fs-TAS measurement of PTQ10:*m*-BTP-PhC6 binary blends without/with different additives: (a)–(c) pseudo 2D color plots. (d)–(f) Spectral linecuts at the indicated pump–probe delay times. The samples were excited using an 800 nm fs-laser with 3 μJ cm^{-2} fluence.

3370 | *Energy Environ. Sci.*, 2024, **17**, 3365–3374

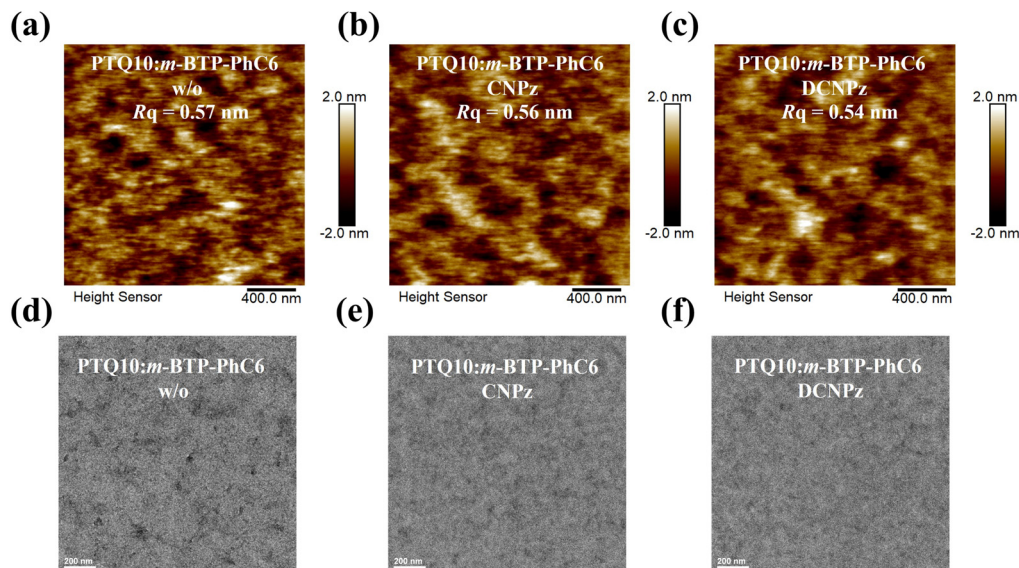This journal is © The Royal Society of Chemistry 2024

Fig. 6 AFM height images of without (a), CNPz (b), and DCNPz (c)-treated PTQ10:*m*-BTP-PhC6 blend films. TEM images of without (d), CNPz (e), and DCNPz (f)-processed PTQ10:*m*-BTP-PhC6 blend films.

indicating that additives barely impact the aggregation of *m*-BTP-PhC6 chain segments. The absorption profiles of the blend films are shown in Fig. 7(f)–(h). After blending with PTQ10:*m*-BTP-PhC6, compared to the control blend film, the CNPz-processed blend film showed increased ordered phase; however, the DCNPz-processed blend film resulted in a decreased ratio of order phase, which explained well the GIWAXS

measurements. To gain more insight into the mechanism of solid additive assisted morphology formation, *in situ* UV/Vis absorption measurements were conducted for all the blend films. The absorptions along with thermal annealing time are observed for these PTQ10:*m*-BTP-PhC6 blends (Fig. S23, ESI†).[70–73]

The results from GIWAXS provide insight into the crystallinity of the blend films, while the grazing incidence small
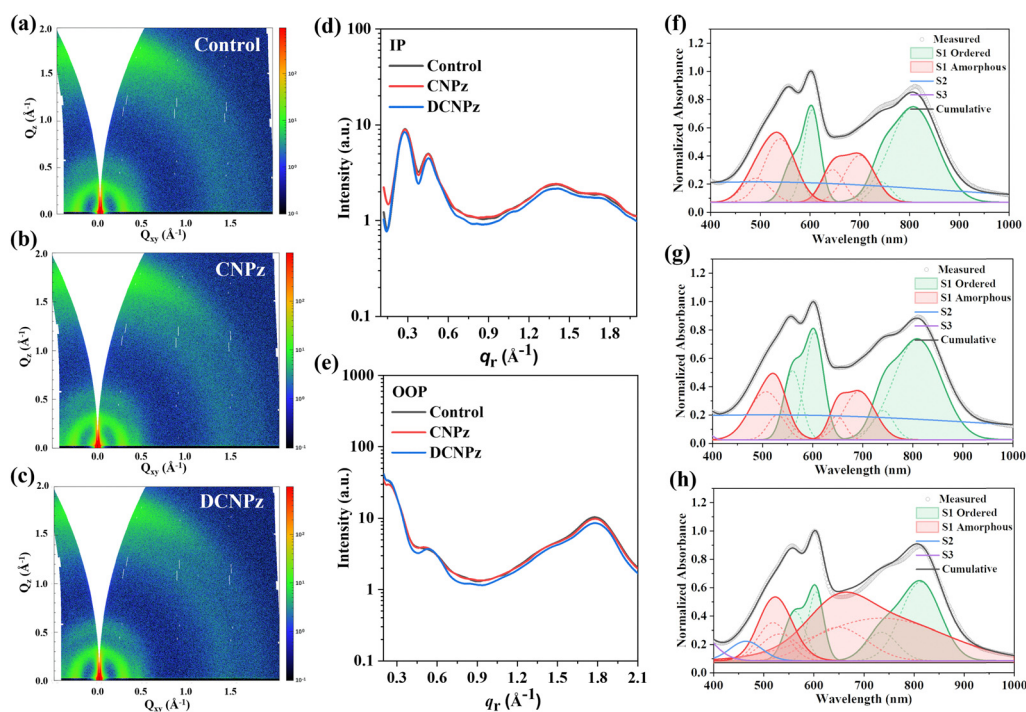

Fig. 7 2D GIWAXS patterns of PTQ10:*m*-BTP-PhC6 blend films: (a) control, (b) with CNPz additive and (c) with DCNPz additive. (d) and (e) The out-of-plane and in-plane line cut of the 2D GIWAXS data. Absorption profiles of PTQ10:*m*-BTP-PhC6 blend films without additive (f), with CNPz additive (g), and with DCNPz additive (h). White hollow point: experiment results; green shaded areas: ordered phase, red shaded areas: amorphous phase; dashed lines indicate vibronic sub-bands.

This journal is © The Royal Society of Chemistry 2024

Energy Environ. Sci., 2024, **17**, 3365–3374 | **3371**

angle X-ray scattering (GISAXS) sheds light on the nanoscale structure (Fig. S24, ESI†). The fitted data reveal ξ values, signifying the average correlation length of the polymer domain, of 41.8, 30.9, and 43.2 nm for the control, CNPz, and DCNPz-treated films, respectively. The pure-phase domain size ($2R_g$) values are 32.6, 21, and 40 nm for the control, CNPz, and DCNPz-treated films. The small $2R_g$ in the CNPz-processed blend film is beneficial to exciton dissociation and transport.

Fig. S25 (ESI†) elucidates the potential mechanism of the solid additives. Upon the incorporation of solid additive, due to the good miscibility and electrostatic interactions, the solid additive can form an intermediate mixture with PTQ10 and m-BTP-PhC6 in the blend films, thus facilitating the π–π stacking. During the annealing process, the solid additive that is attached to PTQ10 and m-BTP-PhC6 would volatilize, thus achieving improved molecular packing, which is beneficial to the charge transfer process, contributing to the J_{SC} and FF.

To verify the generality of the CNPz and DCNPz additives, several common donor/acceptor systems (PM6:L8-BO, PM6:BO-4Cl, and PM6:PY-IT) are chosen to fabricate OSCs. The corresponding J–V and EQE curves are shown in Fig. S26–S28 (ESI†), and the photovoltaic parameters are summarized in Tables S8–S10 (ESI†). All OSCs demonstrate improved FF with CNPz treatment, contributing to a higher PCE than that of the control device. In the CNPz processed PM6:L8-BO systems, the OSC device offers an outstanding PCE of 18.56%, which is higher than 17.69% for the control devices. The excellent general applicability of CNPz further emphasizes its significant potential for achieving high performance OSCs through tuning the nanoscale morphology of the active layers.

Conclusion

In summary, we develop a feasible and efficient strategy to boost the photovoltaic performance by introducing the electron-deficient building blocks, CNPz and DCNPz, as solid additives into the active layer. It is found that CNPz has a more significant dipole moment and enhances intermolecular interaction within the PTQ10:m-BTP-PhC6 blend. Importantly, the CNPz-processed blend film facilitates a compact molecular packing and enhanced crystallinity, promoting exciton dissociation and charge collection. Consequently, a PCE of 19.67% is achieved with the consistent improvement of the J_{SC} of 27.20 mA cm^{-2} and FF of 81.8%, which are much higher than the control device (18.73%). This work provides valuable insights into designing and selecting electron-deficient units as additives for high-performance OSC.

Conflicts of interest

There are no conflicts to declare.

Acknowledgements

References

1 J. Zhang, H. S. Tan, X. Guo, A. Facchetti and H. Yan, *Nat. Energy*, 2018, **3**, 720–731.
2 C. Yan, S. Barlow, Z. Wang, H. Yan, A. K. Y. Jen, S. R. Marder and X. Zhan, *Nat. Rev. Mater.*, 2018, **3**, 18003.
3 C. Li, J. Zhou, J. Song, J. Xu, H. Zhang, X. Zhang, J. Guo, L. Zhu, D. Wei, G. Han, J. Min, Y. Zhang, Z. Xie, Y. Yi, H. Yan, F. Gao, F. Liu and Y. Sun, *Nat. Energy*, 2021, **6**, 605–613.
4 Y. Bai, Z. Zhang, Q. Zhou, H. Geng, Q. Chen, S. Kim, R. Zhang, C. Zhang, B. Chang, S. Li, H. Fu, L. Xue, H. Wang, W. Li, W. Chen, M. Gao, L. Ye, Y. Zhou, Y. Ouyang, C. Zhang, F. Gao, C. Yang, Y. Li and Z.-G. Zhang, *Nat. Commun.*, 2023, **14**, 2926.
5 S. Li, M. Gao, K. Zhou, X. Li, K. Xian, W. Zhao, Y. Chen, C. He and L. Ye, *Adv. Mater.*, 2023, 2307278.
6 Y. Kan, Y. Sun, Y. Ren, Y. Xu, X. Jiang, H. Shen, L. Geng, J. Li, P. Cai, H. Xu, K. Gao and Y. Li, *Adv. Mater.*, 2024, 2312635.
7 Y. Hu, J. Wang, C. Yan and P. Cheng, *Nat. Rev. Mater.*, 2022, **7**, 836–838.
8 D. Qiu, H. Zhang, C. Tian, J. Zhang, L. Zhu, Z. Wei and K. Lu, *Adv. Mater.*, 2023, **35**, 2307398.
9 X. Yang, R. Sun, Y. Wang, M. Chen, X. Xia, X. Lu, G. Lu and J. Min, *Adv. Mater.*, 2022, **35**, 2209350.
10 Y. Sun, Y. Li, Q. Li, Y. Cai, H. Jin, J. Zhang, Z. Tang, C. Zhang and Z. Wei, *Energy Environ. Sci.*, 2022, **15**, 3854–3861.
11 G. Zhang, F. R. Lin, F. Qi, T. Heumüller, A. Distler, H.-J. Egelhaaf, N. Li, P. C. Y. Chow, C. J. Brabec, A. K. Y. Jen and H.-L. Yip, *Chem. Rev.*, 2022, **122**, 14180–14274.
12 P. Cheng, G. Li, X. Zhan and Y. Yang, *Nat. Photonics*, 2018, **12**, 131–142.
13 Y. Lin, J. Wang, Z.-G. Zhang, H. Bai, Y. Li, D. Zhu and X. Zhan, *Adv. Mater.*, 2015, **27**, 1170–1174.
14 J. Yuan, Y. Zhang, L. Zhou, G. Zhang, H.-L. Yip, T.-K. Lau, X. Lu, C. Zhu, H. Peng, P. A. Johnson, M. Leclerc, Y. Cao, J. Ulanski, Y. Li and Y. Zou, *Joule*, 2019, **3**, 1140–1151.
15 Y. Wei, J. Yu, L. Qin, H. Chen, X. Wu, Z. Wei, X. Zhang, Z. Xiao, L. Ding, F. Gao and H. Huang, *Energy Environ. Sci.*, 2021, **14**, 2314–2321.
16 L. Nian, Y. Kan, K. Gao, M. Zhang, N. Li, G. Zhou, S. B. Jo, X. Shi, F. Lin, Q. Rong, F. Liu, G. Zhou and A. K. Y. Jen, *Joule*, 2020, **4**, 2223–2236.
17 Y. Ma, M. Zhang, S. Wan, P. Yin, P. Wang, D. Cai, F. Liu and Q. Zheng, *Joule*, 2020, **5**, 197–209.
18 Z. Bo, Y.-N. Chen, M. Li, Y. Wang, J. Wang, M. Zhang, Y. Zhou, J. Yang, Y. Liu, F. Liu, Z. Tang and Q. Bao, *Angew. Chem., Int. Ed.*, 2020, **59**, 22714–22720.
19 Q. Liu, Y. Jiang, K. Jin, J. Qin, J. Xu, W. Li, J. Xiong, J. Liu, Z. Xiao, K. Sun, S. Yang, X. Zhang and L. Ding, *Sci. Bull.*, 2020, **65**, 272–275.
20 R. Ma, H. Li, T. A. Dela Peña, X. Xie, P. W.-K. Fong, Q. Wei, C. Yan, J. Wu, P. Cheng, M. Li and G. Li, *Adv. Mater.*, 2023, 2304632.

3372 | *Energy Environ. Sci.*, 2024, **17**, 3365–3374

This journal is © The Royal Society of Chemistry 2024

21 M. Du, A. Tang, J. Yu, Y. Geng, Z. Wang, Q. Guo, Y. Zhong, S. Lu and E. Zhou, *Adv. Energy Mater.*, 2023, **13**, 2302429.

22 X. Li, A. Tang, H. Wang, Z. Wang, M. Du, Q. Guo, Q. Guo and E. Zhou, *Angew. Chem., Int. Ed.*, 2023, **62**, e202306847.

23 X. Liu, Z. Zhang, C. Wang, C. Zhang, S. Liang, H. Fang, B. Wang, Z. Tang, C. Xiao and W. Li, *Angew. Chem., Int. Ed.*, 2024, **63**, e202316039.

24 H. Wang, C. Cao, H. Chen, H. Lai, C. Ke, Y. Zhu, H. Li and F. He, *Angew. Chem., Int. Ed.*, 2022, **61**, e202201844.

25 Y. Yu, Y. Zhang, J. Miao, J. Liu and L. Wang, *CCS Chem.*, 2022, **5**, 486–496.

26 X. Yuan, H. Chen, S. Kim, Y. Chen, Y. Zhang, M. Yang, Z. Chen, C. Yang, H. Wu, X. Gao, Z. Liu and C. Duan, *Adv. Energy Mater.*, 2023, **13**, 2204394.

27 J. Wang, P. Xue, Y. Jiang, Y. Huo and X. Zhan, *Nat. Rev. Chem.*, 2022, **6**, 614–634.

28 J. Wang, J. Zhang, Y. Xiao, T. Xiao, R. Zhu, C. Yan, Y. Fu, G. Lu, X. Lu, S. R. Marder and X. Zhan, *J. Am. Chem. Soc.*, 2018, **140**, 9140–9147.

29 K. Liu, Y. Jiang, G. Ran, F. Liu, W. Zhang and X. Zhu, *Joule*, 2024, **8**, 835–851.

30 Y. Cui, Y. Xu, H. Yao, P. Bi, L. Hong, J. Zhang, Y. Zu, T. Zhang, J. Qin, J. Ren, Z. Chen, C. He, X. Hao, Z. Wei and J. Hou, *Adv. Mater.*, 2021, **33**, 2102420.

31 C. He, Y. Pan, Y. Ouyang, Q. Shen, Y. Gao, K. Yan, J. Fang, Y. Chen, C.-Q. Ma, J. Min, C. Zhang, L. Zuo and H. Chen, *Energy Environ. Sci.*, 2022, **15**, 2537–2544.

32 L. Zhu, M. Zhang, J. Xu, C. Li, J. Yan, G. Zhou, W. Zhong, T. Hao, J. Song, X. Xue, Z. Zhou, R. Zeng, H. Zhu, C.-C. Chen, R. C. I. MacKenzie, Y. Zou, J. Nelson, Y. Zhang, Y. Sun and F. Liu, *Nat. Mater.*, 2022, **21**, 656–663.

33 R. Ma, X. Jiang, J. Fu, T. Zhu, C. Yan, K. Wu, P. Müller-Buschbaum and G. Li, *Energy Environ. Sci.*, 2023, **16**, 2316–2326.

34 B. Zou, W. Wu, T. A. Dela Peña, R. Ma, Y. Luo, Y. Hai, X. Xie, M. Li, Z. Luo, J. Wu, C. Yang, G. Li and H. Yan, *Nano-Micro Lett.*, 2023, **16**, 30.

35 L. Guo, Q. Li, J. Ren, Y. Xu, J. Zhang, K. Zhang, Y. Cai, S. Liu and F. Huang, *Energy Environ. Sci.*, 2022, **15**, 5137–5148.

36 L. Zhu, M. Zhang, W. Zhong, S. Leng, G. Zhou, Y. Zou, X. Su, H. Ding, P. Gu, F. Liu and Y. Zhang, *Energy Environ. Sci.*, 2021, **14**, 4341–4357.

37 X. Xu, Y. Li and Q. Peng, *Adv. Mater.*, 2022, **34**, 2107476.

38 Z. Luo, H. Yan and C. Yang, *Acc. Mater. Res.*, 2023, **4**, 968–981.

39 T. Liu, R. Ma, Z. Luo, Y. Guo, G. Zhang, Y. Xiao, T. Yang, Y. Chen, G. Li, Y. Yi, X. Lu, H. Yan and B. Tang, *Energy Environ. Sci.*, 2020, **13**, 2115–2123.

40 N. Nakao, M. Saito, T. Mikie, T. Ishikawa, J. Jeon, H. D. Kim, H. Ohkita, A. Saeki and I. Osaka, *Adv. Sci.*, 2023, **10**, 2205682.

41 G. Zhang, H. Ning, H. Chen, Q. Jiang, J. Jiang, P. Han, L. Dang, M. Xu, M. Shao, F. He and Q. Wu, *Joule*, 2021, **5**, 931–944.

42 Y. Shi, H. Guo, J. Huang, X. Zhang, Z. Wu, K. Yang, Y. Zhang, K. Feng, H. Y. Woo, R. Ortiz, M. Zhou and X. Guo, *Angew. Chem., Int. Ed.*, 2020, **59**, 14449–14457.

43 S. Chen, L. Hong, M. Dong, W. Deng, L. Shao, Y. Bai, K. Zhang, C. Liu, H. Wu and F. Huang, *Angew. Chem., Int. Ed.*, 2023, **62**, e202213869.

44 K. C. Dickey, J. E. Anthony and Y. L. Loo, *Adv. Mater.*, 2006, **18**, 1721–1726.

45 B. Liu, W. Xu, R. Ma, J.-W. Lee, T. A. Dela Peña, W. Yang, B. Li, M. Li, J. Wu, Y. Wang, C. Zhang, J. Yang, J. Wang, S. Ning, Z. Wang, J. Li, H. Wang, G. Li, B. J. Kim, L. Niu, X. Guo and H. Sun, *Adv. Mater.*, 2023, **35**, 2308334.

46 K. Hu, C. Zhu, K. Ding, S. Qin, W. Lai, J. Du, J. Zhang, Z. Wei, X. Li, Z. Zhang, L. Meng, H. Ade and Y. Li, *Energy Environ. Sci.*, 2022, **15**, 4157–4166.

47 X. Liao, Q. He, G. Zhou, X. Xia, P. Zhu, Z. Xing, H. Zhu, Z. Yao, X. Lu and Y. Chen, *Chem. Mater.*, 2020, **33**, 430–440.

48 M. Xiao, Y. Meng, L. Tang, P. Li, L. Tang, W. Zhang, B. Hu, F. Yi, T. Jia, J. Cao, C. Xu, G. Lu, X. Hao, W. Ma and Q. Fan, *Adv. Funct. Mater.*, 2023, 2311216.

49 Z. Gan, L. Wang, J. Cai, C. Guo, C. Chen, D. Li, Y. Fu, B. Zhou, Y. Sun, C. Liu, J. Zhou, D. Liu, W. Li and T. Wang, *Nat. Commun.*, 2023, **14**, 6297.

50 W. Liang, L. Chen, Z. Wang, Z. Peng, L. Zhu, C. H. Kwok, H. Yu, W. Xiong, T. Li, Z. Zhang, Y. Wang, Y. Liao, G. Zhang, H. Hu and Y. Chen, *Adv. Energy Mater.*, 2024, 2303661.

51 G. Han and Y. Yi, *Acc. Chem. Res.*, 2022, **55**, 869–877.

52 L. Chen, J. Yi, R. Ma, L. Ding, T. A. Dela Peña, H. Liu, J. Chen, C. Zhang, C. Zhao, W. Lu, Q. Wei, B. Zhao, H. Hu, J. Wu, Z. Ma, X. Lu, M. Li, G. Zhang, G. Li and H. Yan, *Adv. Mater.*, 2023, **35**, 2301231.

53 S. Bao, H. Yang, H. Fan, J. Zhang, Z. Wei, C. Cui and Y. Li, *Adv. Mater.*, 2021, **33**, 2105301.

54 R. Yu, H. Yao, L. Hong, Y. Qin, J. Zhu, Y. Cui, S. Li and J. Hou, *Nat. Commun.*, 2018, **9**, 4645.

55 Z. Chen, H. Yao, J. Wang, J. Zhang, T. Zhang, Z. Li, J. Qiao, S. Xiu, X. Hao and J. Hou, *Energy Environ. Sci.*, 2023, **16**, 2637–2645.

56 R. Yu, H. Yao, Y. Xu, J. Li, L. Hong, T. Zhang, Y. Cui, Z. Peng, M. Gao, L. Ye, Z. A. Tan and J. Hou, *Adv. Funct. Mater.*, 2021, **31**, 2010535.

57 M. Dong, S. Chen, L. Hong, J. Jing, Y. Bai, Y. Liang, C. Zhu, T. Shi, W. Zhong, L. Ying, K. Zhang and F. Huang, *Nano Energy*, 2024, **119**, 109097.

58 Y. Ran, C. Liang, Z. Xu, W. Jing, X. Xu, Y. Duan, R. Li, L. Yu and Q. Peng, *Adv. Funct. Mater.*, 2023, 2311512.

59 J. Zhao, S. Chung, H. Li, Z. Zhao, C. Zhu, J. Yin, K. Cho and Z. Kan, *Adv. Funct. Mater.*, 2023, **33**, 2307355.

60 L. Xu, Y. Xiong, S. Li, W. Zhao, J. Zhang, C. Miao, Y. Zhang, T. Zhang, J. Wu, S. Zhang, Q. Peng, Z. Wang, L. Ye, J. Hou and J. Wang, *Adv. Funct. Mater.*, 2024, 2314178.

61 L. Kong, Z. Zhang, N. Zhao, Z. Cai, J. Zhang, M. Luo, X. Wang, M. Chen, W. Zhang, L. Zhang, Z. Wei and J. Chen, *Adv. Energy Mater.*, 2023, **13**, 2300763.

62 H. Zhang, G. Ran, X. Cui, Y. Liu, Z. Yin, D. Li, X. Ma, W. Liu, H. Lu, R. Liu, L. Cai, W. Zhang, S. Guo, H. Li, J. Yu, Y. Lin, Y. Liu, G. Lu, Z. Ma, P. Cheng and Z. Bo, *Adv. Energy Mater.*, 2023, **13**, 2302063.

63 H. Lu, K. Chen, R. S. Bobba, J. Shi, M. Li, Y. Wang, J. Xue, P. Xue, X. Zheng, K. E. Thorn, I. Wagner, C.-Y. Lin, Y. Song, W. Ma, Z. Tang, Q. Meng, Q. Qiao, J. M. Hodgkiss and X. Zhan, *Adv. Mater.*, 2022, **34**, 2205926.

This journal is © The Royal Society of Chemistry 2024

Energy Environ. Sci., 2024, **17**, 3365–3374 | **3373**

64 Z. Ling, M. I. Nugraha, W. T. Hadmojo, Y. Lin, S. Y. Jeong, E. Yengel, H. Faber, H. Tang, F. Laquai, A.-H. Emwas, X. Chang, T. Maksudov, M. Gedda, H. Y. Woo, I. McCulloch, M. Heeney, L. Tsetseris and T. D. Anthopoulos, *ACS Energy Lett.*, 2023, **8**, 4104–4112.

65 L. Tu, J. Wang, Z. Wu, J. Li, W. Yang, B. Liu, S. Wu, X. Xia, Y. Wang, H. Y. Woo and Y. Shi, *Angew. Chem., Int. Ed.*, 2024, **63**, e202319658.

66 J.-H. Dou, Y.-Q. Zheng, Z.-F. Yao, Z.-A. Yu, T. Lei, X. Shen, X.-Y. Luo, J. Sun, S.-D. Zhang, Y.-F. Ding, G. Han, Y. Yi, J.-Y. Wang and J. Pei, *J. Am. Chem. Soc.*, 2015, **137**, 15947–15956.

67 H. Zheng, Y. Sang, K. N. Houk, X.-S. Xue and J.-P. Cheng, *J. Am. Chem. Soc.*, 2019, **141**, 16046–16056.

68 C. Bannwarth, S. Ehlert and S. Grimme, *J. Chem. Theory Comput.*, 2019, **15**, 1652–1671.

69 T. A. Dela Peña, R. Ma, Z. Xing, Q. Wei, J. I. Khan, R. M. Young, Y. Hai, S. A. Garcia, X. Zou, Z. Jin, F. L. Ng, K. L. Yeung, D. F. Swearer, M. R. Wasielewski, J. Wang, H. Cha, H. Yan, K. S. Wong, G. Li, M. Li and J. Wu, *Energy Environ. Sci.*, 2023, **16**, 3416–3429.

70 Y. Cho, B. Lee, S. Jung, S. Jeong, J. Park, G. Park, S. Yang and C. Yang, *Energy Environ. Sci.*, 2023, **16**, 6035–6045.

71 L. Zhong, Z. Sun, S. Lee, S. Jeong, S. Jung, Y. Cho, J. Park, J. Park, S.-J. Yoon and C. Yang, *Adv. Funct. Mater.*, 2023, **33**, 2305450.

72 J. Oh, S. Jung, S.-H. Kang, G. Park, M. Jeong, S. Kim, S. Lee, W. Kim, B. Lee, S. M. Lee and C. Yang, *J. Mater. Chem. A*, 2022, **10**, 20606–20615.

73 Y. Zhang, Y. Cho, J. Lee, J. Oh, S.-H. Kang, S. M. Lee, B. Lee, L. Zhong, B. Huang, S. Lee, J.-W. Lee, B. J. Kim, Y. Li and C. Yang, *J. Mater. Chem. A*, 2020, **8**, 13049–13058.